Ocean Sci. Discuss., 10, 2399–2432, 2013
www.ocean-sci-discuss.net/10/2399/2013/
doi:10.5194/osd-10-2399-2013

Ocean Science
Discussions
Open Access

Hydrographic situation during cruise M84/3 and P414 (spring 2011) in the Mediterranean Sea

D. Hainbucher[1], A. Rubino[2], V. Cardin[3], T. Tanhua[4], K. Schroeder[5], and M. Bensi[1]

[1]CEN, Institut für Meereskunde, University of Hamburg, Bundesstraße 53, 20146 Hamburg, Germany
[2]Università Ca' Foscari di Venezia, Dorsoduro, 2137 – C.A.P. 30121, Italy
[3]OGS – Istituto Nazionale di Oceanografia e di Geofisica Sperimentale, Borgo Grotta Gigante 42/c, 34018 Sgonico, Trieste, Italy
[4]GEOMAR Helmholtz Centre for Ocean Research Kiel, Department of Chemical Oceanography, Düsternbrooker Weg 20, 24105 Kiel, Germany
[5]Istituto di Scienze Marine – ISMAR, Consiglio Nazionale delle Ricerche (CNR), Arsenale – Tesa 104, Castello 2737/F, 30122 Venice, Italy

Received: 16 October 2013 – Accepted: 1 December 2013 – Published: 16 December 2013

Correspondence to: D. Hainbucher (dagmar.hainbucher@zmaw.de)

Published by Copernicus Publications on behalf of the European Geosciences Union.

Abstract

Hydrography and large scale circulation observed in the Mediterranean Sea during the M84/3 and P414 cruises (April and June 2011, respectively) are presented. In contrast to most of the recent expeditions, which were limited to special areas of the basin, these two cruises, especially the M84/3, offered the opportunity of delineating a quasi-synoptic picture of the distribution of the relevant physical parameters through the whole Mediterranean. A section was observed from the Lebanese coast up to the Strait of Gibraltar. The focus of our analysis are the water mass properties, also in the context of the recently observed variability, and a comparison between the velocity fields observed using a vessel-mounted ADCP and those calculated from the observed density fields. Overall, a distribution of temperature, salinity, and geostrophic velocities emerges, which seems far from that observed before the beginning of the so-called "Eastern Mediterranean Transient", a major climatic shift in the hydrography and circulation of the Mediterranean Sea occurred at the end of 1980s. Here, our focus is a discussion of the observed water mass properties analysed through T–S diagrams and through an Optimum Multiparameter (OMP) analysis. Additionally, ADCP velocities are compared to geostrophic calculations.

1 Introduction

The Euroafrican Mediterranean Sea is a marginal sea, as it is separated from the Atlantic Ocean through the narrow Strait of Gibraltar. It consists of two sub- basins, the Western (WMed) and the Eastern (EMed) Mediterranean, which communicate through the broad (145 km) and shallow (maximum depth at its western sill is 550 m) Sicily Channel. It represents a natural barrier for the inter-basin circulation of intermediate and deep waters. As a consequence, which adds to the differences in bathymetry as well as forcings existing between the two sub-basins, the WMed and EMed show distinct differences both in their hydrographic conditions and circulation.

OSD
10, 2399–2432, 2013

Different attempts, based on observational evidences, to schematize surface as well as intermediate and deep paths of circulation of the Mediterranean Sea have been made in the past (e.g., POEM Group, 1992; Malanotte-Rizzoli et al., 1997, 1999; Robinson et al., 2001; Roether et al., 2007; Schroeder et al., 2012).

The surface layer in the WMed is dominated by the inflow of relatively low-salinity Atlantic Water (AW) through the Strait of Gibraltar. This water mass is subject to different, mostly wind-driven currents that coexist with a complex path of circulation in a general cyclonic manner and only a fraction of it enters the EMed through the Sicily Channel. The intermediate layer is occupied by the Levantine Intermediate Water (LIW) originated in the EMed, and whose core is found typically between 200 and 400 m depth. The abyssal water mass in the WMed, produced by shelf and open-ocean convection is the Western Mediterranean Deep Water (WMDW), which is formed in the Gulf of Lyons (Leaman and Schott, 1991).

In the EMed, the AW, the Levantine Surface Water (LSW) and the Ionian Surface Water (ISW) dominate the surface layer (approximately down to 100 m depth). In the intermediate layer the LIW is clearly associated with the salinity maximum found typically between 50 and 600 m depth. Its importance for the oceanography and climatology of the Mediterranean Sea is large: formed in the Levantine Sea and in the Rhodes Gyre (Özturgut, 1976) it is able to flow through the Sicily Channel into the WMed and thus represent the intermediate water mass connection between the two basins. Additionally, more regionally confined water masses, like the Cretan Intermediate Water (CIW) can be found in the intermediate layer of the EMed (Robinson et al., 2001). The Adriatic Deep Water (AdDW) and water of Aegean origin named Cretan Deep Water (CDW) (Schlitzer et al., 1991) are deep water masses and are produced in the two deep water formation regions of the EMed. Thus, the predominant water mass of the bottom layers filling the abyssal plains of the Ionian and Levantine basins is the Eastern Mediterranean Deep Water (EMDW) being a mixture of AdDW, CDW and surrounding water masses.

OSD
10, 2399–2432, 2013

Concerning the basin long-term variability, one has to note that, since 1960, the WMed has experienced a marked long-term warming and salinification trend in its deep water (Béthoux et al., 1990). Possibly, such a trend has started well before, but the accuracy of the available observations does not allow for a statistically significant reconstruction. These variations have been mostly attributed to changes in climate. Very intense deep water formation events occurred since 2005 (Schroeder et al., 2008) with the consequence that the deep waters of the WMED have experienced significant physical changes (Lopez-Jurado et al., 2005; Schroeder et al., 2006, 2008): an abrupt increase in the deep heat and salt contents and a dramatic change in the deep stratification, with the appearance of sharp inversions in the temperature-salinity diagrams.

Similarly the EMed run through most dramatic changes in hydrography and circulation during the last decades. These drastic changes are known as the Eastern Mediterranean Transient (EMT, see Roether et al., 1996). Together with the occurrence of anomalous meteorological, oceanic, and hydrological phenomena, the source of the EMDW shifted abruptly from the Adriatic Sea to the Aegean Sea (see e.g. Roether et al., 1996; Klein et al., 1999; Lascaratos et al., 1999). As a consequence, the characteristics of the EMDW changed dramatically and resulted in a new, rapidly and still evolving thermohaline circulation.

In this study we present aspects of hydrography and large scale circulation observed in the Mediterranean Sea during cruises M84/3 and P414 (April and June 2011, respectively). Our focus is a discussion of the observed water mass properties analysed through T–S diagrams and through an Optimum Multiparameter (OMP) analysis. Additionally, ADCP velocities are compared to geostrophic calculations. The distribution of salinity, temperature and density along the section occupied by the M84/3 cruise carried out in 2011 are shown by Tanhua et al. (2013b).

OSD
10, 2399–2432, 2013

2 Data and methods

Since the EMT started at the end of the 1980s a lot of surveys were carried out in the Mediterranean to monitor the evolution of the hydrography, circulation and biogeochemistry (POEM, 1988; POEM-BC, 1996; LIWEX, 2003; BOUM, 2008, etc.), but most of them were restricted to special areas. METEOR cruise M84/3 constitutes an exception as it is one of very few recent cruises (another one was the BOUM cruise, Moutin et al., 2012), carried out after the appearance of the EMT, which ran on a section across the whole Mediterranean Sea with the goal of producing a synoptic picture of the distribution of relevant physical and chemical properties in both basins. Furthermore, it re-occupied relevant stations of previous surveys, most importantly the METEOR survey M5/6 in 1987, which provided the last picture of the situation before the EMT. POSEIDON cruise P414 (2011) was designed to complete M84/3, with stations especially in the southern Adriatic and northern Ionian Sea. One major goal of that cruise was to observe the overflow of dense water of Adriatic origin in the Ionian basin, with the purpose of monitoring the effects of the thermohaline changes observed in the Adriatic on the EMDW (Bensi et al., 2013a). Both cruises were designed to follow the lines of the GO-SHIP Program (Global Ocean Ship Based Hydrographic Investigation Program, www.go-ship.org), which aims at creating a globally coordinated network of sustained hydrographic sections as part of the global ocean/climate observing system. Besides acquiring data for a nearly synoptic picture of the water mass property distribution across the whole Mediterranean Sea, the data collected by these two cruises can be used to determine changes in the circulation and in the distribution of properties and thereby fill in the gaps in the knowledge of the Mediterranean system.

More information about the cruises can be found in Tanhua et al. (2013a) and Hainbucher (2012).

OSD
10, 2399–2432, 2013

2.1 Conductivity-temperature-depth (CTD)/rosette and hydrographic samples

Altogether, 61 full depth standard hydrographic stations were sampled during cruise M84/3 (Fig. 1a) and 33 full depth standard hydrographic stations during cruise P414 (Fig. 1b). A SeaBird SBE911plus CTD-O_2 probe equipped with dual sensors of temperature, salinity and oxygen was employed attached to a SeaBird carousel 24 (12) bottle water sampler during the M84/3 (P414) together with an altimeter. Additionally, a fluorometer sensor was installed on the CTD during the M84/3 cruise and a digital reversing thermometer was attached to the probe for calibration purposes.

At almost all stations water samples for dissolved oxygen were taken at different depths throughout the whole water column. Dissolved oxygen from bottle samples were analysed on board using a Winkler potentiometric method. A detailed description of oxygen sampling and distribution during cruise M84/3 can be found in Tanhua et al., 2013a and b. Dissolved oxygen is relevant in the discussion here only in the context of the applied OMP analysis.

From three depth levels, depending on the vertical profile of the stations, water samples were taken also for salinity analysis for calibration purposes and they were analyzed onboard using a Guildline Autosal Salinometer.

Temperature, salinity and pressure data were post-processed by applying Seabird software and MATLAB routines. Spikes were removed, 1 dbar averages calculated, and temperature, salinity, and dissolved oxygen corrected with a regression analysis which fits the downcast profiles with the temperature, salinity and DO. Since the corrections applied to these parameters were small, the data quality can be considered excellent. Overall accuracies are within expected ranges: 0.002 °C for temperature, 0.003 for salinity and 2 % of saturation for dissolved oxygen. Additionally, we calculated potential temperature with the appropriate MATLAB routines. We always refer to potential temperature in case we use the term temperature in our discussions and figures.

OSD
10, 2399–2432, 2013

2.2 Acoustic Doppler Current Profiler (ADCP) velocity measurements

A vessel mounted ADCP (Teledyne RD Instruments) 38 kHz (with bin size of 32 m) was used during the M84-3 cruise. On P414 cruise we used an ADCP (Teledyne RD Instruments) 75 kHz ADCP (with bin size of 8 m). Both worked in narrowband mode. The data were post-processed with the software package ossi14 (ocean surveyor sputum interpreter), developed by the Leibniz Institute of Marine Sciences, Kiel, which also corrects for the misalignment angle. An objective quality control of the data was impossible to be performed as no data for comparison or correction (like additional lADCP data) were available.

2.3 Quantification of water mass fractions

The mixing of water masses and their spatial distributions in the western and eastern Mediterranean Sea were determined using the OMP (Optimum Multiparameter) analysis developed by Tomczak (1981) and described in detail in Tomczak and Large (1989). To apply this method we assume that all hydrographic parameters are conserved and therefore not influenced by biogeochemical processes. This assumption also holds for dissolved oxygen as our analysis is conducted over a limited region and the rather restricted temporal scales of the involved advective-diffusive processes prevail over biochemically induced concentration changes (Leffanue and Tomczak, 2004; Manca et al., 2006). The OMP method is essentially based on establishing a linear system of n equations from observations of $n-1$ parameters and from the equation of mass conservation, and by deriving the contribution of the n water types to a given water sample as the exact solution to the n equations.

The method bears two challenges: the determination of parameter weights and the determination of water types. As described in Cardin et al. (2011) and in Kovačević et al. (2012), who applied the method to the Adriatic Sea and to the Ionian Sea, respectively, the weight for each parameter was derived as follows: the variance of each parameter of the considered water masses was calculated within the relevant vertical

OSD
10, 2399–2432, 2013

water layer and for the relevant stations. The largest variance of the same parameter among the considered water masses is represented by v2. The variance (v1) of the overall mean (the average of the considered different mean values associated with the different water masses) is determined. The ratio between v1 and v2 represents the weight, i.e. the relevance of each parameter used in the calculation. Some additional adjustments are made to equal salinity and mass conservation weights to that of temperature after normalization (to sum of 100) of the values. The weights reflect the degree of conservativeness of each parameter, measurement accuracy and other processes which may render some parameters less reliable than others (Tomczak and Large, 1989). Therefore, temperature and salinity (and mass conservation) always obtain the largest weights. For our OMP analysis we additionally added oxygen values, as this parameter possesses the same vertical resolution as temperature and salinity due to the fact that it was measured through CTD sensors. Note that, because high weights are obtained for temperature and salinity, other parameters unavoidably exert a smaller influence on the OMP results. The results for weights came up as follows: temperature, salinity and conservation of mass equals 33 and oxygen equals 1.

In the Mediterranean Sea the water mass definitions are broadly diversified and the definition of their characteristics differs often to some extent, presumably due to location and time when the water mass was found. Ideally, properties of water types are defined in the source region and reasonably back in time, which certainly is not possible for most of all hydrographical investigations due to lack of data. Therefore, in our study water mass properties were determined with the help of T–S diagrams, profiles and the knowledge about typical water mass distributions in the Mediterranean Sea, under the assumption that these water masses are climatologic mean quantities. The characteristics are listed in Table 1. Depending on season and location, as already stated, the properties of the water masses can vary distinctly. Table 2 specifies temperature and salinity values found in literature for the relevant water masses (Roether et al., 1998; Millot, 1999; Lascaratos et al., 1999; Teocharis et al., 1999; Gertman et al., 2006; Schroeder et al., 2006; Kovačević et al., 2012; Bensi et al., 2013a, b).

OSD
10, 2399–2432, 2013

In the WMed we generally find 4 major water masses (Fig. 2a, panel a): Modified Atlantic Water (MAW) in the surface layer, LIW in the intermediate layer, and old and new WMDW from mid depths down to the bottom. Our definition for MAW in the WMed results from the T–S profiles of station 334, which is close to the entrance of the Strait of Gibraltar, where we find a pronounced salinity minimum in the surface layer. The definition of LIW for the WMed is given by the T–S profiles of station 320, which is close to the Channel of Sicily, where we find the salinity maximum at about 350 m depth. As known, WMDW is a mixture of water masses resulting from deep convection in the Gulf of Lions. Old and new WMDW were determined by considering the values encountered in the hook like T–S structures of Fig. 6b and c: new WMDW is slightly warmer and saltier than older WMDW, and more oxygenated. Thus, for the OMP analysis we focus on these 4 main water masses.

For the EMed we also revert to the basic source water masses: MAW, LSW for the surface layers, LIW for the intermediate layers and AdDW and CDW for the bottom layers (Fig. 2a, panel b).

MAW was defined according to the profiles of stations 304/305 where we found the salinity minimum in around 100 m depth. The locations of these stations were closest to the Sicily Channel where MAW enters the EMed. For LSW we considered the T–S characteristics at the surface of station 287, which is located in the Aegean Sea. Note that LSW is usually predominant during summer with much higher temperature values than those found during these cruises at the beginning of the summer season. LIW was defined according to station 296 located in the centre of the Levantine basin, where we found the salinity maximum at $\sim$170 m depth. We assume that the EMDW, which we also found during our cruises, results from the mixing of AdDW and CDW and therefore it is not taken into account for the OMP analyses. AdDW is defined according to the profiles collected in the Strait of Otranto and CDW according to the profiles collected in the Kasos Strait.

OSD
10, 2399–2432, 2013

2.4 Geostrophic velocities

Using pressure, temperature, and salinity data, geostrophic velocities have been calculated for cross-sections through the western and eastern Mediterranean Sea. The reference layer of no motion was set to 1000 m depth because the use of deeper layers of no motion did not change the results substantially. Note that the distance between stations was too large to resolve any mesoscale features in the velocity distributions. These are limited by the Rossby radius of deformation which is of the order of 10–15 km in the Mediterranean Sea (Robinson et al., 2001).

3 Analysis and discussion

3.1 Water mass properties and vertical distribution

To define the water mass properties and their major transformations during the M84/3 and P414 cruises, potential temperature/salinity diagrams (T–S) constructed for different layer depths and regions are considered. Figure 2b gives an overview of the T–S characteristics in the whole Mediterranean Sea during spring measured in April and June 2011. Notice, that all figures reflect the hydrographic situation during spring. The T–S diagram highlights the differences which exist between the EMed and WMed. Overall, in the EMed, excluding the surface layer down to 50 m, values vary in a relatively small salinity range (between 38.4 and 39.1, i.e., there is a difference of 0.7) and in a relatively large temperature range (between 13.0 °C and 18.2 °C, i.e. there is a difference of 5.2 °C). In contrast, in the WMed the values vary in a much broader salinity range (from about 36.4 to 38.7, i.e., there is a difference of 2.3), but in a relatively narrow temperature range (from about 12.9 °C to 15.9 °C, i.e., there is a difference of 3 °C). Sea water properties close to the bottom are also quite different in the two sub-basins: salinity and temperature values are much larger in the EMED (comprise between 13.4 °C–13.64 °C and 38.72–38.79) than in the WMed (12.87 °C–13.29 °C

OSD
10, 2399–2432, 2013

and 38.46–38.58). As a consequence, bottom density reaches values $\sigma_0 \sim 29.3\,\mathrm{kg\,m^{-3}}$ ($\sigma_2 \sim 37.81\,\mathrm{kg\,m^{-3}}$) in the EMed and $\sigma_0 \sim 29.1\,\mathrm{kg\,m^{-3}}$ ($\sigma_2 \sim 37.75\,\mathrm{kg\,m^{-3}}$) (i.e., about 0.2 (0.06) $\mathrm{kg\,m^{-3}}$ smaller) in the WMed.

Figure 3 highlights the differences between LIW properties in the WMed and EMed. In the EMed, the LIW enters the Ionian sea through the Cretan passage spreading from its formation sites (northeastern Levantine Sea and Rhodes cyclonic gyre; Ovchinnnikov, 1984; Malanotte-Rizzoli & Hech, 1988; Lascaratos, 1993) towards west and it is identified by a salinity maximum encountered at ~50–100 m (in the Levantine Sea) or ~200–400 m (in the Ionian Sea). From our data it can be seen that in the EMed LIW values range between 38.85 and 39.3 and 14.6 °C and 17.8 °C. In the WMed, where the LIW enters through the Sicily Channel and crosses with an initially westward and northward trajectory, less salty (values between 38.45 and 38.75) and cooler (values between 14.1 °C and 13 °C) characteristics are encountered. This fact is due to its progressive dilution with the ambient waters during its way towards the Strait of Gibraltar. Nevertheless, it maintains a constant density due to compensation between the thermohaline parameters.

The densest water found during the two cruises (Fig. 4) was in the Aegean Sea (St. 288). It was characterized by $\sigma_0 > 29.3\,\mathrm{kg\,m^{-3}}$, $T_{\mathrm{Pot}} \approx 13.95\,^{\circ}\mathrm{C}$, and $S \approx 39.06$, and thus it corresponded to the CDW. This fact is not unusual and not relevant as long as the amount of water is not massive and deep enough to cross the ridge. The densest water of Adriatic origin, instead, was characterized by $\sigma_0 < 29.3\,\mathrm{kg\,m^{-3}}$, $T_{\mathrm{Pot}} \approx 13.02\,^{\circ}\mathrm{C}$, and $S \approx 38.74$ (St. 303). However, comparing the dense water outflow in the Strait of Otranto, the outflow region of Adriatic Deep Water, with that in the Kasos Strait, the outflow region of CDW, we found denser water in the Strait of Otranto (σ_0 distinctly $> 29.2\,\mathrm{kg\,m^{-3}}$, $T_{\mathrm{Pot}} \approx 13.25\,^{\circ}\mathrm{C}$, and $S \approx 38.73$). The water in Kasos Strait reached values of $\sigma_0 \approx 29.2\,\mathrm{kg\,m^{-3}}$, $T_{\mathrm{Pot}} \approx 14.43\,^{\circ}\mathrm{C}$ and, $S \approx 39.04$ (see Fig. 4).

According to Roether et al. (2007) the anomalously abundant and dense water outflow of Aegean origin during the EMT produced a noticeable increase of temperature and salinity throughout the EMed deep waters. Especially in the Levantine basin and

OSD
10, 2399–2432, 2013

in the Hellenic Trench, this increase could be detected as a long-lasting, pronounced T–S inversion (Roether et al., 2013). Indeed, during M84/3 we still can find this inversion in a broad area of the Levantine basin (Fig. 5a). There, T–S values are distributed closely together, with their minima being located at about 1000 m depth. In the deeper stations (excluding the easternmost 3 stations) a T–S maximum is reached at about 2200 m depth, followed by a steadily T and S decrease. In the eastern Hellenic Trench (Fig. 5b) the T–S distribution is similar, but the minima are found at about 1300–1700 m depth and the maxima at about 1800–2100 m depth. The salinity difference between the extreme values is much larger in the Levantine than in the eastern Hellenic Trench. Compared to the distributions found by Roether et al. (2007) during the EMT, the shape of the T–S diagrams changed slightly. During the latter this intermediate maxima were not found in the Levantine basin, but T and S increased steadily in the deep layer, after reaching their minimum. Only in the Hellenic Trench shapes characterized by intermediate minima and maxima were found. Also the depth of the inversions changed. While during the EMT the inversions took place in a layer between 1000–1700 m, this feature can now be found in a wider layer.

During the EMT, this kind of shape of the T–S diagram ("peaking") was prominent in the Ionian Sea only in the northern part of the Eastern Mediterranean Ridge, the principal entrance for water of Aegean origin (Roether et al., 2007). Remarkably, now it can be found in the whole Ionian Sea (Fig. 5b), but it is characterized by a much less pronounced range between minima and maxima. In general, the T–S range between stations is small. The inversions are also less pronounced in the Ionian Sea than in the Levantine and Hellenic Trench. The depths of the inversions lay between 1200 and 1900 m, the corresponding density level being $\sigma_0 = 29.18\,\mathrm{kg\,m^{-3}}$ ($\sigma_2 = 37.88\,\mathrm{kg\,m^{-3}}$), which corresponds to the same density level encountered in the Levantine basin. For the deep stations an additional near-bottom minimum can be found in about 3000 m depth. Salinity is 38.73 in P414, and 38.72 in M84/3 (station 306). Note that salinity increases close to the bottom, while temperature remains constant at 13.42 °C.

OSD
10, 2399–2432, 2013

Presumably, this minimum corresponds to a branch of old EMDW of Adriatic origin (Bensi et al., 2013a).

The stations in the western Hellenic Trench show a more scattered distribution. It seems that, especially the P414 stations 362 (black) and 361 (red) and the M84-3 station 300 (cyan) are under the influence of the Antikithera outflow in the upper layers. We note an increase in salinity from April 2011 (M84/3) to June 2011 (P414), which confirms the more direct response of this region to the outflow. In the deepest station (blue) we find a minimum in T and S close to the bottom. Hence, it can also be assumed that here the influence of the AdDW on the EMDW was strong.

Since 2005 the deep waters of the WMed experienced significant physical changes (Schroeder et al., 2006; Font et al., 2009). Probably, the major change corresponds to an abrupt increase in the deep heat and salt content. This increase appears like a "hook" in the deep T–S diagrams which arises from the interaction between old deep water, new deep water formed by open-sea convection and dense shelf cascading water (Salat et al., 2009). The data collected during the M84/3 cruise clearly show the presence of this "hook"-like pattern (Fig. 6b and c). In these data, the minimum is located at a depth of about 1200–1600 m, with temperature values of about 12.87–12.89 °C and salinity values of about 38.46–38.48. The differences between the minimum values and the values at the bottom are small: in T and S <= 0.01 °C/psu respectively. The new WMDW is still missing in the Tyrrhenian Sea (Fig. 6a), because of the sill at 1900 m that separates this subbasin from the rest of the WMed. Here, the T–S diagrams show an almost linear decrease from mid depths to the bottom. Bottom values are higher ($T \approx 13$ °C, $S \approx 38.5$) than in the "hook" shape case even while depths of more than 1600 m are reached.

3.2 Determination of water mass fractions by OMP

Due to the availability of just 3 parameters (T, S, O_2) we had to make several separate OMP runs for the western Mediterranean to calculate the fractions of the 4 relevant

OSD
10, 2399–2432, 2013

water masses. In particular we determined the relation between MAW-LIW-$WMDW_{new}$, MAW-LIW-$WMDW_{old}$, and LIW-$WMDW_{new}$-$WMDW_{old}$.

In all considered OMP cases (Fig. 7a) MAW is encountered as a shallow near-surface lens throughout the whole section. Also the appearance of LIW in the intermediate water column from about 200 to 1000 m with a distinct core at about 500 m in the eastern side of the section (Fig. 7b) can be observed in all OMP cases. All different OMP combinations also reveal WMDW more or less exclusively in the layers beneath 1000 m but it is not clear which kind of WMDW, new or old one, is the predominant. Depending on the OMP case sometimes the old and sometimes the new WMDW fraction is prevailing (Fig. 7c and d as examples).

In case of the eastern Mediterranean we considered as well three parameters for our OMP analyses. Again, to compensate this limitation we carried out different runs to determine the relative importance of the water masses. One run was focussed on the upper 500 m of the water column. Here we combined MAW with LSW and LIW. All other runs considered the water column from 500 m to the bottom. We combined LIW with AdDW and CDW, MAW with LIW and AdDW. LSW is dominant in the eastern and central part of the section in the upper 200 m (Fig. 8a) while LIW is predominant in the intermediate layers throughout the section whereas it forms different cores in depths between 100 and 300 m (Fig. 8b). The different OMP runs for the deep water masses AdDW and CDW produce qualitatively more or less the same results. AdDW fills the basins from 1000 m to the bottom (Fig. 8d), but with decreasing percentages towards the east where CDW contributes to about 30 % of the deep water (Fig. 8c).

Summarizing our results, we can conclude that, for the EMed, the hydrographic situation which we found during the two cruises reveals for the upper ocean a well known situation with LSW at the surface and LIW in the intermediate layers. The situation beneath is dominated by water masses originating from the Adriatic Sea, which confirms the assumption that after the EMT, and in particular after 2003, AdDW returned to be the main water mass for deep water formation in the EMed (Rubino and Hainbucher, 2007; Bensi et al., 2013a). The high amount of AdDW which we found even in the

OSD
10, 2399–2432, 2013

Levantine basin in 2011 together with the fact that the turnover times in the EMed are longer than decades queries the overall importance of AdDW for the deep water formation in the EMed over longer time-scales. This is supported by a recent study by Roether et al. (2013) that found no evidence of EMT like events during the observational record.

3.3 Geostrophic and mean ADCP velocities

There are remarkable differences between the geostrophic velocities of the WMed and EMed. Peak velocities (maximum and minimum) are distinctly higher in the WMed than in the EMed, but the structures do not reach as deep and are not as wide as in the EMed. In the former (Fig. 9a) the features reach down to about 200 m depth, are of the order of 100 km width, and reach maximum amplitudes of ~ 12–$15\,\mathrm{cm\,s^{-1}}$. Differently, maximum velocities in the EMed are $\sim 5\,\mathrm{cm\,s^{-1}}$ and the features widths are about 300–400 km (Fig. 10a). These structures might be related to sub-basin scale gyres, this assumption being supported by the range of the features and the changing appearance of positive and negative amplitudes. In the EMed the velocity feature is correlated with the Mersa-Matruh anticyclone (Tanhua et al., 2013, this issue Fig. 2).

In order to compare the ADCP velocities with the results of the geostrophic calculations, the ADCP data collected between two consecutive CTD stations were averaged. The along track velocities were determined and the velocities across the sections are presented in Figs. 9b and 10b. In the EMed there were data gaps and often the track between CTD stations was not direct, so that part of the ADCP data could not be considered for our calculation: only 7 significant CTD stations remained, which were taken into account for applying the method.

Altogether, large velocity amplitudes are achieved mainly in the upper 500 m of the water column in both basins. Beneath this water depth current speeds are around 1–$2\,\mathrm{cm\,s^{-1}}$. For the WMed, geostrophic velocities and mean ADCP velocities agree well. Structures and amplitudes are similar and the ageostrophic fraction (Fig. 9c) determined by subtracting the geostrophic velocity from the ADCP velocity is comparably

OSD
10, 2399–2432, 2013

low. This leads to the assumption that in the WMed large scale velocities in the upper part of the ocean are mainly determined by geostrophy, while in the EMed the situation is opposite. Again, largest velocities are reached in the area of the Mersa-Matruh anticyclonic gyre. They far exceed the geostrophic velocity with maximum amplitudes of more than 12 cm s^{-1} (Fig. 10c), indicating that the ageostrophic fraction in the EMed circulation is dominating the velocity distribution.

4 Summary and conclusion

In the EMed the typical post-EMT temperature and salinity inversions were found in the deep waters throughout the whole region, still indicating an increase in property distribution. *T*–*S* diagrams show that the AdDW returned to represent the main source for the EMDW. However, it became much saltier and warmer than before the EMT. It is also the dominating water filling the deeper basins of the EMed, whereas CDW is limited to a shallower layer (approximately around 2000 m) in the proximity of Kasos Strait. In the upper layer of the EMed, LIW is prevailing in the intermediate layers, MAW is dominant in the western part of the EMed and LSW in the eastern regions. The velocity distribution derived by the ADCP measurements and geostrophic calculations indicates that in the EMed the ageostrophic component of the velocity is dominating. Relevant velocity amplitudes can only be found in the upper 500 m of the water column.

In the WMed the situation in the deep layers is dominated by the "hook" shape of the *T*–*S* distribution, indicating a transition in bottom waters between old and new WMDW. One exception is represented by the situation found in the Tyrrhenian Sea, where temperature and salinity did not reach the range where the "hook" case occurs. In the deep layers WMDW is filling the basin, but from our results we cannot discern if the new or the old WMDW is the predominant one. In the upper layers MAW is predominant in the surface layers, whereas LIW is filling the intermediate depth levels with a core in the eastern part of the WMed. In contrast to the EMed, the velocity is here

OSD
10, 2399–2432, 2013

more geostrophically balanced and the structures observed can be related to known sub-basin scale gyres.

The salinity range in the WMed is larger than in the EMed, certainly due to input of fresher water of Atlantic origin. On the other hand, the temperature range in both regions is of the same order. Bottom densities of the WMed are lower than in the EMed and are determined by salinity decreases. On the contrary, LIW is lighter in the EMed and the mean depth at which LIW flows deepens from east to west.

Overall, we can conclude that the hydrographic property distribution which we found during April–June 2011 in the western and eastern Mediterranean Sea characterizes a situation which is far from that observed before the EMT. Likely, the effects induced by the EMT are still evident in the Mediterranean Sea, and considering the time delay of many years which characterizes oceanographic processes on a basin scale, we could expect that they still will be present for some time.

Acknowledgement. The authors want to thank the captains and crews on the research vessels RV *Meteor* and RV *Poseidon* for the excellent cooperation during the campaigns. Thanks go to all scientists involved in the field campaigns. Special thanks go to Norbert Verch for processing and calibrating the hydrographic data of both cruises.

The Meteor cruise M84/3 was supported by a grant from the Deutsche Forschungsgemenschaft – Senatskommision fur Ozenographie (DFG), and from a grant from the DFG; TA 317/3-1. The Poseidon cruise 414 was supported by funding from the University of Hamburg.

References

Bensi, M., Rubino, A., Cardin, V., Hainbucher, D., and Mancero-Mosquera, I.: Structure and variability of the abyssal water masses in the Ionian Sea in the period 2003–2010, J. Geophys. Res., 118, 1–13, doi:10.1029/2012JC008178, 2013a.

Bensi, M., Cardin, V., Rubino, A., Notarstefano, G., and Poulain, P. M.: Effects of winter convection on the deep layer of the Southern Adriatic Sea in 2012, J. Geophys. Res.-Ocean, 118, 6064–6075, doi:10.1002/2013JC009432, 2013b.

OSD

10, 2399–2432, 2013

Bethoux, J. P., Gentili, B., Raunet, J., and Taillez, D.: Warming trend in the Western Mediterranean deep water, Nature, 347, 660–662, 1990.

Cardin, V., Bensi, M., and Pacciaroni, M.: Variability of water mass properties in the last two decades in the South Adriatic Sea with emphasis on the period 2006–2009, Cont. Shelf Res., 31, 951–965, 2011.

Font, J., Béranger, K., Bryden, H., Budillon, G., Fuda, J. L., Gaèiæ, M., Gascard, J. C., Packard, T., Puig, P., Roether, W., Salat, J., Salusti, E., Schroeer, K., Theocharis, A., and van Haren, H.: Executive summary of CIESM workshop 38 "Dynamics of Mediterranean deep waters", in: CIESM, 2009, Dynamics of Mediterranean Deep Waters, N°38 in CIESM Workshop Monographs, edited by: Briand, F., Monaco, 132 pp., 2009.

Gertman, I., Pinardi, N., Popov, Y., and Hecht, A.: Aegean Sea water masses during the early stages of the Eastern Mediterranean Climatic Transient (1988–1990), J. Phys. Oceanogr. 36, 1841–1859, 2006.

Hainbucher, D.: Cruise Report RV POSEIDON Cruise P414, available at: http://www.geomar.de/fileadmin/content/zentrum/ze/fs/Poseidon_Berichte_2011_PDF/POS414_Hainbucher.pdf (last access: 12 December 2013), 2012.

Klein, B., Roether, W., Manca, B. B., Bregant, D., Beitzel, V., Kovačević, V., and Luchetta, A.: The large deep water transient in the Eastern Mediterranean, Deep-Sea Res. Pt. I, 46, 371–414, 1999.

Kovačević, V., Manca, B. B., Ursella, L., Schroeder, K., Cozzi, S., Burca, M., Mauri, E., Gerin, R., Notarstefano, G., and Deponte, D.: Water mass properties and dynamic conditions of the Eastern Mediterranean in June 2007, Prog. Oceanogr., 104, 59–79, 2012.

Lascaratos, A.: Estimation of deep and intermediate water mass formation rates in the Mediterranean Sea, Deep-Sea Res. Pt. II, 40, 1327–1332, 1993.

Lascaratos, A., Roether, W., Nittis, K., and Klein, B.: Recent changes in deep water formation and spreading in the Eastern Mediterranean Sea: a review, Progr. Oceanogr., 44, 5–36, 1999.

Leaman, K. D. and Schott, F.: Hydrographic structure of the convection regime in the Golfe du Lion, J. Phys. Oceanogr., 23, 575–598, 1991.

Leffanue, H. and Tomczak, M.: Using OMP analysis to observe temporal variability in water mass distribution, J. Marine Syst., 48, 3–14, 2004.

OSD
10, 2399–2432, 2013

López-Jurado, J.-L., González-Pola, C., and Vélez-Belchi, P.: Observation of an abrupt disruption of the long-term warming trend at the Balearic Sea, western Mediterranean Sea, in summer 2005, Geophys. Res. Lett., 32, L24606, doi:10.1029/2005GL024430, 2005.
Manca, B. B., Ibello, V., Pacciaroni, M., Scarazzato, P., and Giorgetti, A.: Ventilation of deep waters in the Adriatic and Ionian Seas following changes in thermohaline circulation of the Eastern Mediterranean, Clim. Res., 31, 239–256, 2006.
Malanotte-Rizzoli, P. and Hecht, A.: Large-scale properties of the eastern Mediterranean: a review, Oceanol. Acta, 11, 323–335, 1988.
Malanotte-Rizzoli, P. and Robinson, A. R.: POEM: physical oceanography of the Eastern Mediterranean, EOS T. Am. Geophys. Un., 69, 194–203, 1988.
Malanotte-Rizzoli, P., Manca, B. B., Ribera d'Alcala, M., Teocharis, A., Bergamasco, A., Bregant, D., Budillon, G., Civitarese, G., Georgopoulos, D., Michelato, A., Sansone, E., Scarazzato, P., and Souvermezoglou, E.: A synthesis of the Ionian Sea hydrography, circulation and water mass pathways during POEM-Phase I, Prog. Oceanogr., 39, 153–204, 1997.
Malanotte-Rizzoli, P., Manca, B. B., Ribera d'Alcala, M., Theocharis, A., Brenner, A., Budillon, G., and Ozsoy, E.: The Eastern Mediterranean in the 80s and in the 90s: the big transitino in the intermediate and deep circulations, Dynam. Atmos. Oceans, 29, 365–395, 1999.
Millot, C.: Circulation in the Western Mediterranean Sea, J. Marine Syst., 20, 423–444, 1999.
Moutin, T., Van Wambeke, F., and Prieur, L.: Introduction to the Biogeochemistry from the Oligotrophic to the Ultraoligotrophic Mediterranean (BOUM) experiment, Biogeosciences, 9, 3817–3825, doi:10.5194/bg-9-3817-2012, 2012.
Ovchinnikov, I. M.: Intermediate Water formation in the Mediterranean Sea, Okeanologiya, 24, 217–225, 1984.
Özturgut, E.: The Source and Spreading of the Levantine Intermediate Water in the Eastern Mediteranean, Saclant ASW Research Center Memorandum Sm-92, La Spezia, Italy, 45 pp. 1976.
POEM Group: General circulation of the eastern Mediterranean, Earth-Sci. Rev., 32, 285–309, 1992.
Robinson, A. R., Leslie, W. G., Theocharis, A., and Lascaratos, A.: Mediterranean Sea Circulation Encyclopedia of Ocean Sciences, Academic Press, 1689–1706, 2001.
Roether, W., Manca, B. B., Klein, B., Bregant, D., Georgopoulos, D., Beitzel, V., Kovačević, V., and Lucchetta, A.: Recent changes in Eastern Mediterranean deep waters, Science, 271, 333–335, 1996.

OSD
10, 2399–2432, 2013

Roether, W., Klein, B., Beitzel, V., and Manca, B. B.: Property distributions and transient-tracer ages in Levantine Intermediate water in the Eastern Mediterranean, J. Marine Syst., 18, 71–87, 1998.

Roether, W., Klein, B., Manca, B. B., Theocharis, A., and Kioroglou, S.: Transient Eastern Mediterranean deep waters in response to the massive dense-water output of the Aegean Sea in the 1990s, Prog. Oceanogr., 74, 540–571, 2007.

Roether, W., Klein, B., and Hainbucher, D.: The Eastern Mediterranean transient: evidence for similar events previously?, in: The Mediterranean Sea: Temporal Variability and Spatial Patterns, edited by: Borzelli, G. L. E., AGU monographs, 2013.

Rubino, A. and Hainbucher, D.: A large abrupt change in the abyssal water masses of the eastern Mediterranean, Geophys. Res. Lett., 34, L23607, doi:10.1029/2007GL031737, 2007.

Salat, J., Emelianov, M., and Puig, P.: From bottom water (Lacombe, 1985) to New-WMDW since 2005. Possible shifts on open sea deep convection, in: CIESM, 2009, Dynamics of Mediterranean Deep Waters, N° 38 in CIESM Workshop Monographs, edited by: Briand, F., Monaco, 132 pp., 2009.

Schlitzer, R., Roether, W., Oster, H., Junghans, H.-G., Hausmann, M., and Michelato, A.: Chlorofluoromethane and oxygen in the eastern Mediterrancah, Deep-Sea Res., 38, 1531–1551, 1991.

Schroeder, K., Gasparini, G. P., Tangherlini, M., and Astraldi, M.: Deep and intermediate water in the Western Mediterranean under the influence of the Eastern Mediterranean Transient. Geophys. Res. Lett., 33, L21607, doi:10.1029/2006GL027121, 2006.

Schroeder, K., Ribotti, A., Borghini, M., Sorgente, R., Perilli, A., and Gasparini, G. P. An extensive western Mediterranean deep water renewal between 2004 and 2006, Geophys. Res. Lett., 35, LI8605, doi:10.1029/2008GL035146, 2008.

Schroeder, K., Schroeder, K., Garcìa-Lafuente, J., Josey, S. A., Artale, V., Buongiorno Nardelli, B., Carrillo, A., Gačić, M., Gasparini, G. P., Herrmann, M., Lionello, P., Ludwig, W., Millot, C., Özsoy, E., Pisacane, G., Sánchez-Garrido, J. C., Sannino, G., Santoleri, R., Somot, S., Struglia, M., Stanev, E., Taupier-Letage, I., Tsimplis, M. N., Vargas-Yáñez, M., Zervakis, V., and Zodiatis, G.: Circulation of the Mediterranean Sea and its variability, in: The Climate of the Mediterranean Region: From the Past to the Future, edited by: Lionello, P., Elsevier Insights, Amsterdam, 2012.

OSD
10, 2399–2432, 2013

Tanhua, T., Hainbucher, D., Cardin, V., Álvarez, M., Civitarese, G., McNichol, A. P., and Key, R. M.: Repeat hydrography in the Mediterranean Sea, data from the *Meteor* cruise 84/3 in 2011, Earth Syst. Sci. Data, 5, 289–294, doi:10.5194/essd-5-289-2013, 2013a.

Tanhua, T., Hainbucher, D., Schroeder, K., Cardin, V., Álvarez, M., and Civitarese, G.: The Mediterranean Sea system: a review and an introduction to the special issue, Ocean Sci., 9, 789–803, doi:10.5194/os-9-789-2013, 2013b.

Theocharis, A., Nittis, K., Kontoyiannis, H., Papageorgiou, E., and Balopoulos, E.: Climatic changes in the Aegean Sea influence the Eastern Mediterranean thermohaline circulation (1986–1997), Geophys. Res. Lett., 26, 1617–1620, 1999.

Tomczak, M.: A multiparameter extension of temperature/salinity diagram techniques for the analysis of non-isopycnal mixing, Progr. Oceanogr., 10, 147–171, 1981.

Tomczak, M. and Large, D. G. B.: Optimum multiparameter analysis of mixing in the thermocline of the Eastern Indian Ocean, J. Geophys. Res., 94, C11, 16141–16149, 1989.

OSD

10, 2399–2432, 2013

Table 1. Water masses and their characteristics for (a) the WMed and (b) the EMed. Acronyms used to define water masses: MAW (Modified Atlantic Water), LSW (Levantine Surface Water), LIW (Levantine Intermediate Water), WMDWn (Western Mediterranean Deep Water new), WMDWo (Western Mediterranean Deep Water old), AdDW (Adriatic Deep Water), CDW (Cretan Deep Water).

Water Mass	Temperature (°C)	Salinity	Oxygen ($\mu mol\,kg^{-1}$)
(a) Western Mediterranean Sea:			
MAW	16.39	36.381	230
LIW	14.01	38.726	164
WMDWn	12.905	38.485	185
WMDWo	12.870	38.462	179
(b) Eastern Mediterranean Sea:			
MAW	15.20	38.562	214
LSW	16.85	39.217	216
LIW	16.33	39.180	213
AdDW	13.25	38.730	197
CDW	14.43	39.040	197

OSD
10, 2399–2432, 2013

Table 2. Water masses and their characteristics as they can be found in literature for (a) the WMed and (b) the EMed (Roether et al., 1998, Millot, 1999, Lascaratos et al., 1999, Teocharis et al., 1999, Gertman et al., 2006, Schroeder et al., 2006, Kovačević et al., 2012, Bensi et al., 2013a, b). Ranges of properties are given if possible. Acronyms used to define water masses: MAW (Modified Atlantic Water), LSW (Levantine Surface Water), LIW (Levantine Intermediate Water), WMDWn (Western Mediterranean Deep Water new), WMDWo (Western Mediterranean Deep Water old), AdDW (Adriatic Deep Water), CDW (Cretan Deep Water).

Water Mass	Temperature (°C)	Salinity
(a) Western Mediterranean Sea:		
MAW	> 14	> 36.5
LIW	> 13.1	> 38.47
WMDWn	12.9	38.48
WMDWo	12.75–12.80	38.44–38.46
(b) Eastern Mediterranean Sea:		
MAW	17.7–23.29	37.38–38.10
LSW	17.0–28.0	39.0–39.4
LIW	12.85–14.2	38.37–38.80
AdDW	13.00–13.60	38.663–38.72
CDW	13.66–14.2	38.80–38.95

OSD
10, 2399–2432, 2013

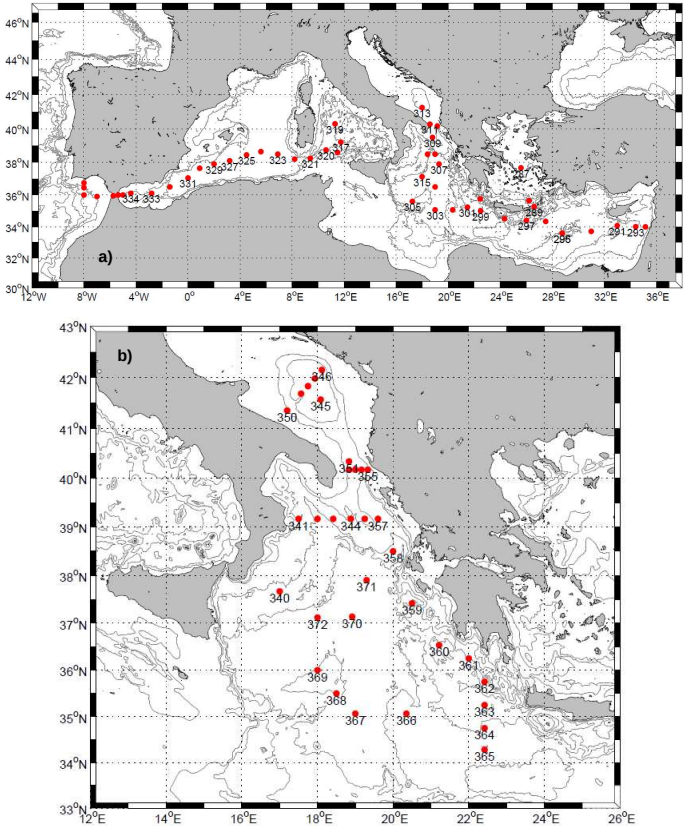

Fig. 1. (a) CTD stations (red dots) of *Meteor* cruise M84-3 during April 2011; **(b)** CTD stations (red dots) of *Poseidon* cruise P414 during June 2011.

OSD
10, 2399–2432, 2013

Hydrographic situation during cruise M84/3 and P414

D. Hainbucher et al.

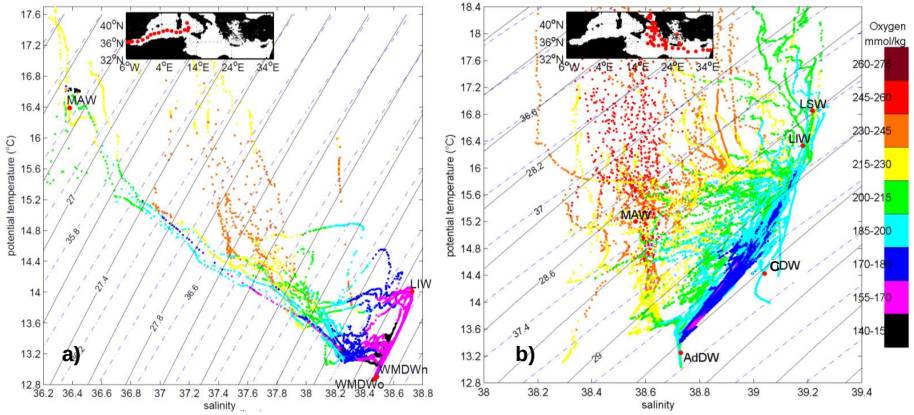

Fig. 2a. *T*–*S* diagrams of the western **(a)** and eastern **(b)** Mediterranean Sea. Colours represent the concentration of oxygen in µmol kg^{-1}. All depth levels from 0 m to bottom are taken into account. The locations of water mass sources are indicated by red dots (MAW = Modified Atlantic Water, LSW = Levantine Surface Water, LIW = Levantine Intermediate Water, WMDW = Western Mediterranean Deep Water, AdDW = Adriatic Deep Water, ADW = Cretan Deep Water). The inner panels show the location of considered stations. Note that scales of *T* and *S* of left and right panel are not identical.

OSD
10, 2399–2432, 2013

Hydrographic situation during cruise M84/3 and P414

D. Hainbucher et al.

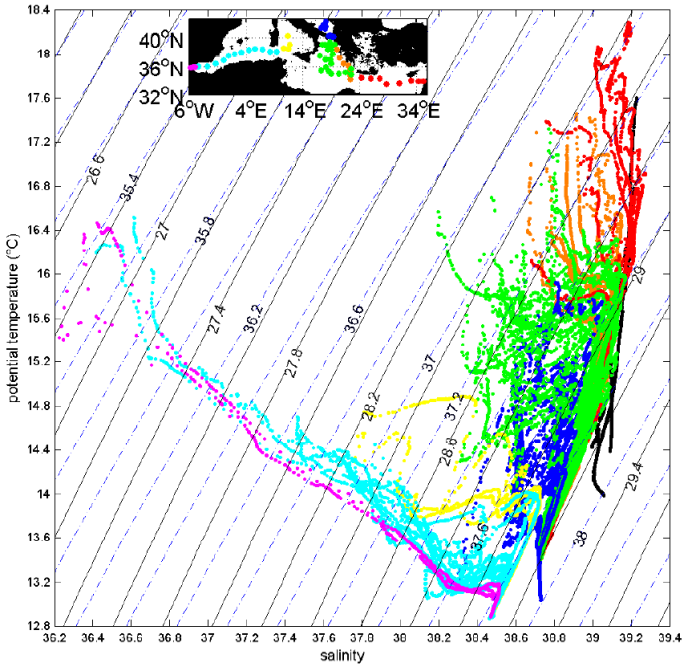

Fig. 2b. T–S diagram of all CTD stations taken during cruise M84-3 and P414 in spring 2011. Values from 50 m depth down to the bottom are considered. Colours show different regions of the Mediterranean Sea. Black dots: Aegean Sea, red dots: Levantine Sea, green dots: Ionian Sea, orange dots: Hellenic Trench, blue dots: Adriatic Sea, yellow dots: Tyrrhenian Sea, cyan dots: remaining western Mediterranean Sea, magenta dots: Strait of Gibraltar. Isolines for potential density $\sigma_0 = \rho_0$ (referenced to sea surface) $-1000\,\mathrm{kg\,m^{-3}}$ (black continuous line) and for potential density $\sigma_2 = \rho_{2000}$ (referenced to 2000 m) $-1000\,\mathrm{kg\,m^{-3}}$ (blue dashed line) are given. Inner panel shows the location of the different stations.

OSD
10, 2399–2432, 2013

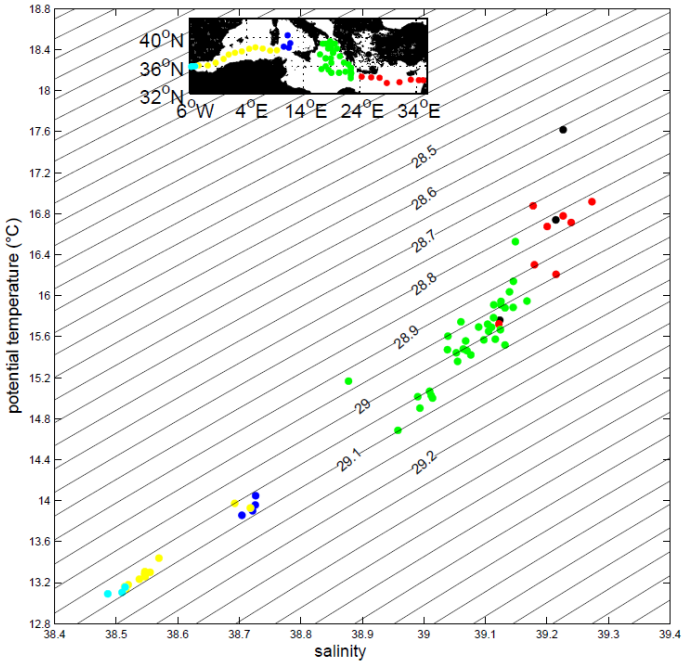

Fig. 3. *T*–*S* diagram of maximum salinity and corresponding temperature in the layer 50–650 m, which shows the LIW core in the Mediterranean Sea. Colours show different regions. Black dots: Aegean Sea, red dots: Levantine Sea, green dots: Ionian Sea, blue dots: Tyrrhenian Sea, yellow dots: remaining western Mediterranean Sea, cyan dots: Strait of Gibraltar. Isolines for potential density $\sigma_0 = \rho_0$ (referenced to sea surface) $-1000\,\mathrm{kg\,m^{-3}}$ (black continuous line) are given. Inner panel shows the location of the different stations.

OSD
10, 2399–2432, 2013

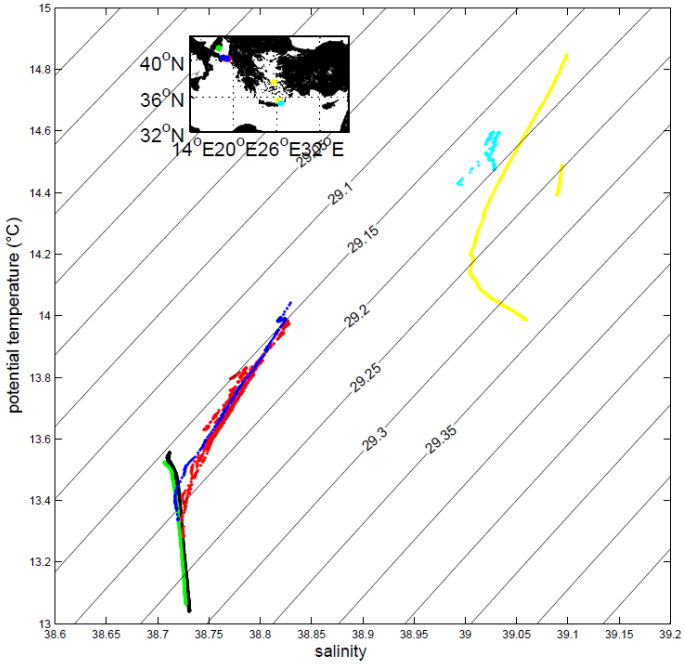

Fig. 4. *T–S* diagram in the areas where dense waters are produced (Aegean and Adriatic Seas). Only values from 600 m to bottom are considered. Yellow dots: Aegean Sea stations of M84-3. Cyan dots: Kasos Strait station of M84-3. Black dots: Adriatic Pit stations of P414. Green dots: Adriatic Pit stations of M84-3 and red dots: Strait of Otranto, stations of P414. Inner panel shows the location of the different stations.

OSD
10, 2399–2432, 2013

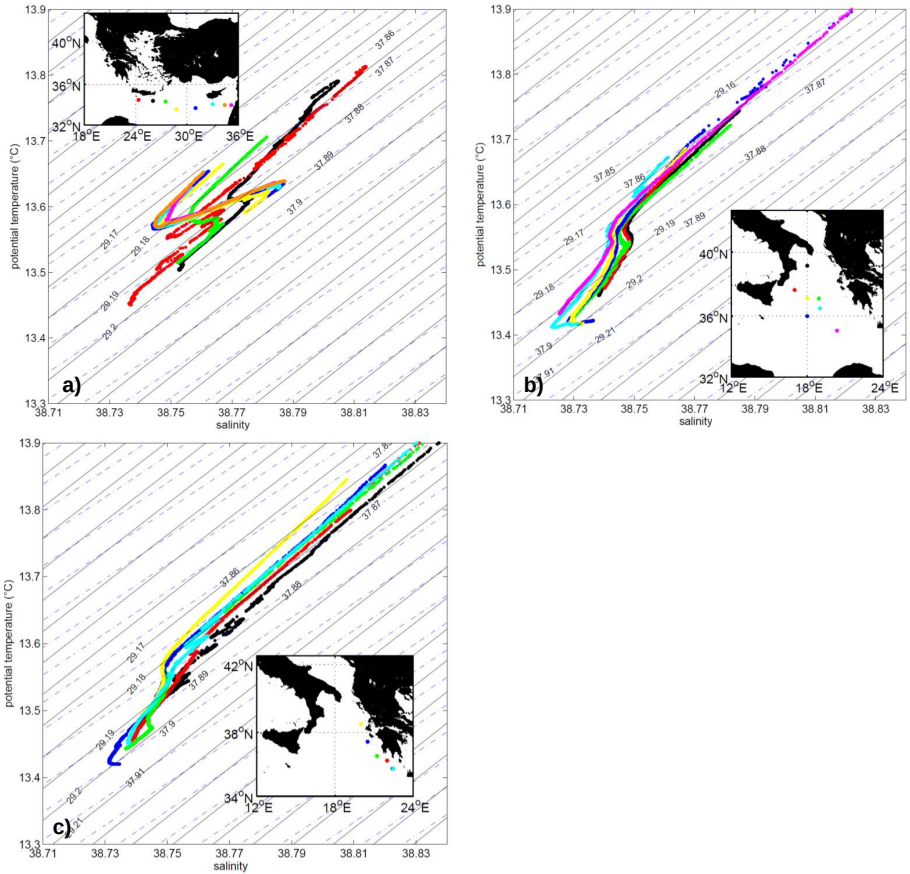

Fig. 5. *T*–*S* diagrams of M84-3 and P414 CTD stations in **(a)** the Levantine basin along the eastern Hellenic Trench, **(b)** in the Ionian basin (for clarity only selected CTD stations are shown) and **(c)** in the western part of the Hellenic Trench. Values from 800 m depth down to the bottom are taken into account. The inner panels show the location of the different stations.

OSD
10, 2399–2432, 2013

Hydrographic situation during cruise M84/3 and P414

D. Hainbucher et al.

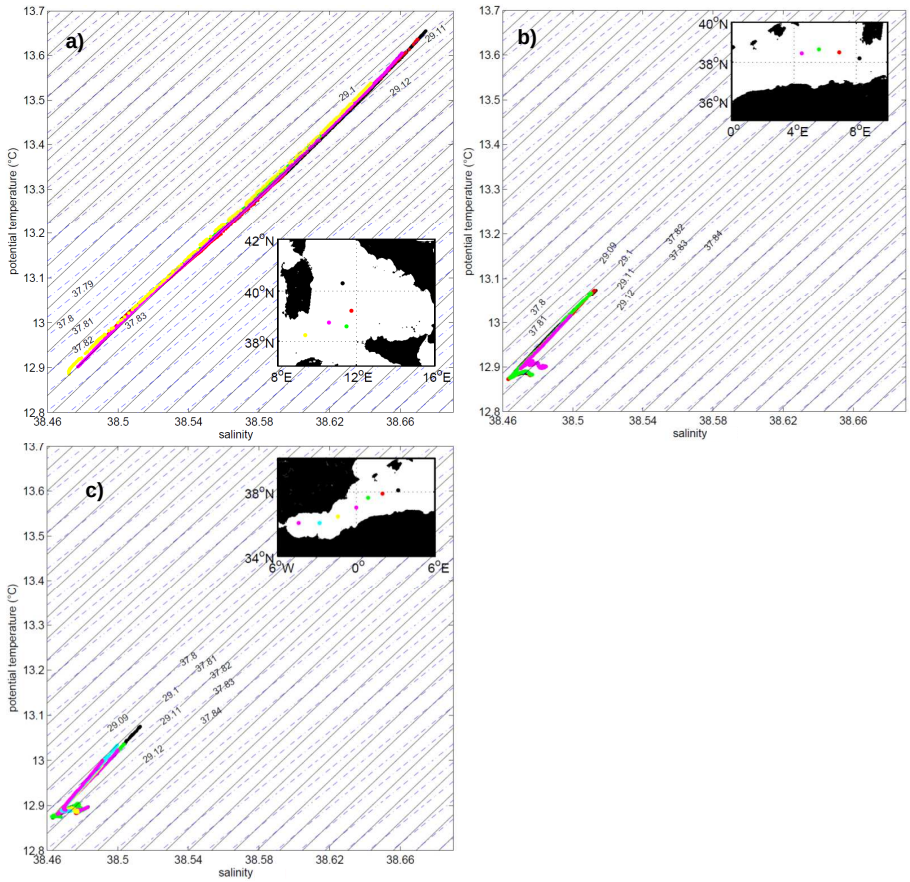

Fig. 6. *T*–*S* diagrams of M84/3 stations in **(a)** the Tyrrhenian Sea, **(b)** the Western Mediterranean Sea between the Balearic Islands and Sardinia and **(c)** the Western Mediterranean Sea between Gibraltar and the Balearic Islands. Values from 800 m depth down to the bottom are taken into account. The inner panels show the location of the different stations.

OSD
10, 2399–2432, 2013

Hydrographic situation during cruise M84/3 and P414

D. Hainbucher et al.

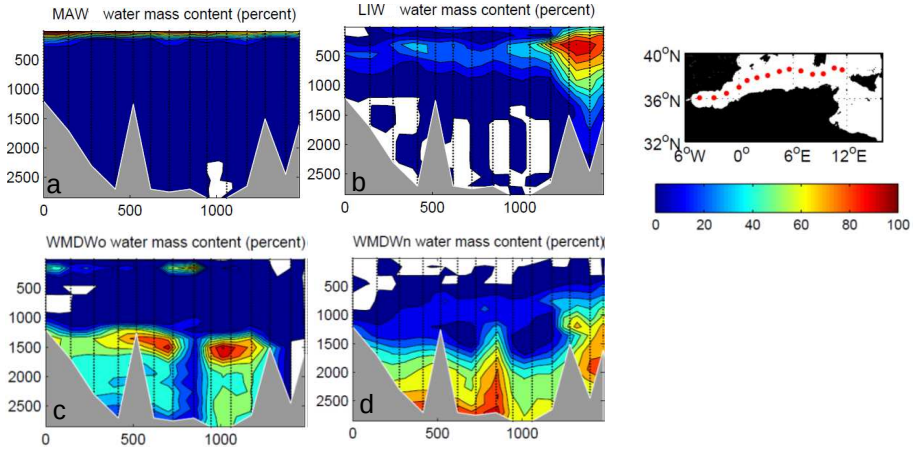

Fig. 7. Water mass fractions in percentage for the western Mediterranean Sea. **(a–b)** show Modified Atlantic Water and Levantine Intermediate Water for the OMP case MAW-LIW-$WMDW_n$. **(c)** shows old Western Mediterranean Deep Water for case MAW-$WMDW_n$-$WMDW_o$ and **(d)** shows new Western Mediterranean Deep Water for case LIW-$WMDW_n$-$WMDW_o$. Y-axes indicate depth in dbar and x-axes specify distance in km. The right panel shows the location of considered stations. White patches are areas for which the OMP method is not valid.

OSD
10, 2399–2432, 2013

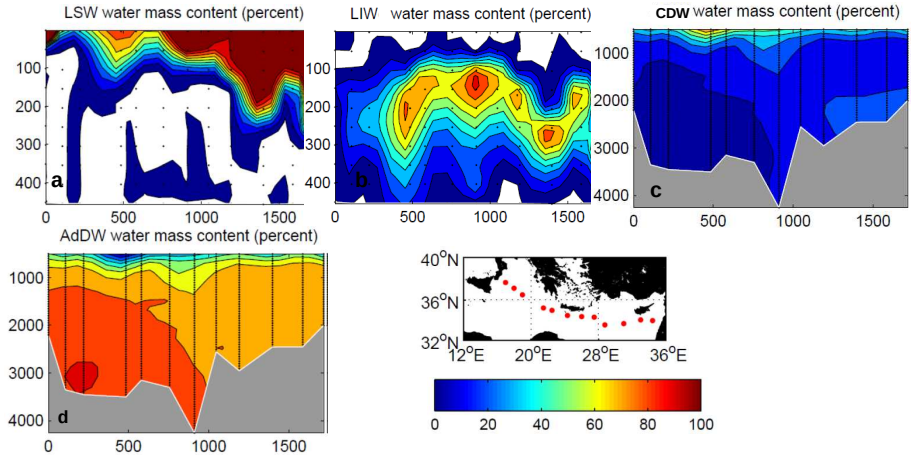

Fig. 8. Water mass fractions in percentage for the eastern Mediterranean Sea. **(a)** Levantine Surface water from surface to 500 m. **(b)** Levantine Intermediate Water from surface to 500 m. Panels a, b result from the OMP run which combines MAW, LSW and LIW in the upper 500 m. **(c)** Cretan Deep water from 500 m to bottom. **(d)** Adriatic Deep Water from 500 m to bottom. Panel c and d result from an OMP combination of MAW, AdDW and CDW from 500 m down to the bottom. Lower right panel: Location of section and colour scale for percentage. Right axis of panels: depth in dbar and lower axis: distance in km. White patches are areas for which the OMP method is not valid.

OSD
10, 2399–2432, 2013

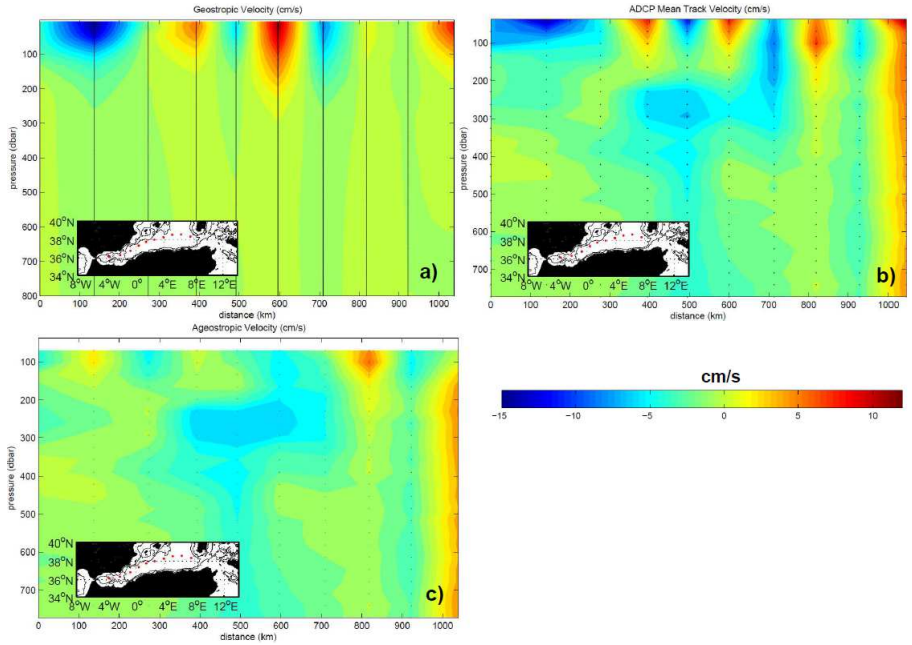

Fig. 9. Velocity distribution on a section through the western Mediterranean Sea. The inner panels show the location and nodes of the section. **(a)** Geostrophic velocity determined between the CTD stations. **(b)** Mean ADCP velocity across the section. Mean are calculated between two CTD stations. **(c)** Ageostrophic velocity determined by subtracting the geostrophic velocity from the mean ADCP velocity. Reference layer of no motion for geostrophic velocities is 1000 m.

OSD
10, 2399–2432, 2013

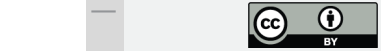

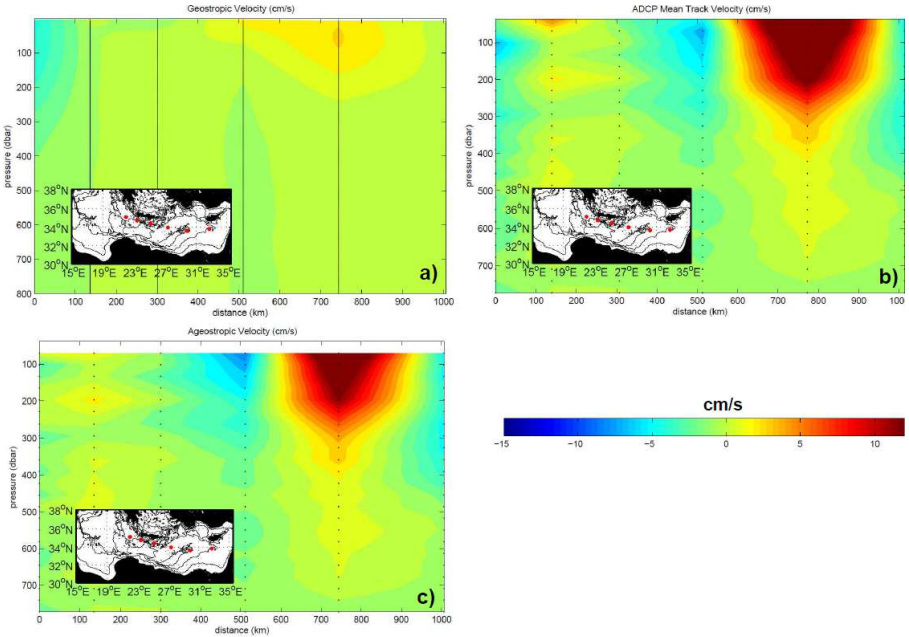

Fig. 10. Velocity distribution on a section through the eastern Mediterranean Sea. The inner panels show the location and nodes of the section. **(a)** Geostrophic velocity determined between the CTD stations. **(b)** Mean ADCP velocity across the section. Mean is the average between two CTD stations. **(c)** Ageostrophic velocity determined by subtracting the geostrophic velocity from the mean ADCP velocity. Reference layer of no motion for geostrophic velocities is 1000 m.

OSD
10, 2399–2432, 2013

Hydrographic situation during cruise M84/3 and P414

D. Hainbucher et al.